online!
www.pnas.org

phys

PROCEEDINGS
OF THE
NATIONAL ACADEMY OF SCIENCES
OF THE UNITED STATES OF AMERICA

April 28, 1998
Volume 95 / Number 9

INCLUDES: NEW POLICY ON RELEASE OF STRUCTURAL COORDINATES
AND LIST OF NEW MEMBERS ELECTED TO THE NATIONAL ACADEMY OF SCIENCES

PHYSICAL SCIENCES LIBRARY
MAY 07 1998

PROCEEDINGS
OF THE
NATIONAL ACADEMY OF SCIENCES
OF THE UNITED STATES OF AMERICA

Officers of the Academy

BRUCE ALBERTS, *President*
JACK HALPERN, *Vice President*
PETER H. RAVEN, *Home Secretary*
F. SHERWOOD ROWLAND, *Foreign Secretary*
RONALD L. GRAHAM, *Treasurer*

Editor-in-Chief

NICHOLAS R. COZZARELLI

Editorial Board of the Proceedings

MAY R. BERENBAUM, PETER J. BICKEL, WILLIAM CATTERALL, ANTHONY CERAMI, PIERRE CHAMBON, MARSHALL H. COHEN, STANLEY N. COHEN, DAVID R. DAVIES, HERMAN N. EISEN, RAYMOND L. ERIKSON, ANTHONY S. FAUCI, NINA FEDOROFF, CHARLES FEFFERMAN, WALTER M. FITCH, JOSEPH L. GOLDSTEIN, CAROL A. GROSS, JACK HALPERN, BERTIL HILLE, PIERRE C. HOHENBERG, H. ROBERT HORVITZ, ALFRED G. KNUDSON, ROGER KORNBERG, ROBERT LANGER, HARVEY F. LODISH, PHIL W. MAJERUS, PHILIPPA MARRACK, ARNO G. MOTULSKY, RONALD L. PHILLIPS, THOMAS D. POLLARD, STANLEY B. PRUSINER, CHARLES RADDING, GIAN-CARLO ROTA, JEREMY A. SABLOFF, PAUL R. SCHIMMEL, STUART L. SCHREIBER, AARON J. SHATKIN, CARLA J. SHATZ, KAI L. SIMONS, CHRISTOPHER A. SIMS, SOLOMON H. SNYDER, CHRISTOPHER R. SOMERVILLE, LARRY R. SQUIRE, CHARLES F. STEVENS, FRANK H. STILLINGER, KARL K. TUREKIAN, DON C. WILEY, PETER G. WOLYNES

Publisher: KENNETH R. FULTON
Managing Editor: DIANE M. SULLENBERGER
Associate Editorial Manager: JOHN M. MALLOY
Associate Manager for Production: JOANNE D'AMICO
Production Coordinator: BARBARA A. BACON
Editorial Coordinator: THOR RUNEMAN
System Administrator: MARILYN J. MASON
Manuscript Coordinator: DANIEL H. SALSBURY
Administrative Assistants: AZADEH FULLMER, JESSAMINE PRICE
Financial Manager: JOSEPH F. RZEPKA, JR.
Financial Assistant: JULIA A. LITTLE
Business and Marketing Assistant: ROBERT J. BENN, JR.
Subscription Fulfillment Assistants: CYNTHIA MATHEWS, MELISSA VALENTINE
Secretary: BRENDA L. MCCOY

PROCEEDINGS OF THE NATIONAL ACADEMY OF SCIENCES OF THE UNITED STATES OF AMERICA (ISSN-0027-8424) is published biweekly by THE NATIONAL ACADEMY OF SCIENCES.

Correspondence: PROCEEDINGS OF THE NATIONAL ACADEMY OF SCIENCES, 2101 Constitution Avenue, NW, Washington, DC 20418 USA (via U.S. postal service) or 1055 Thomas Jefferson Street, NW, Suite FO2013, Washington, DC 20007 USA (via courier or express mail). E-mail: PNAS@nas.edu.

Information for Authors: See pp. xiv–xvi (of this issue) or http://www.pnas.org.

Copyright: Volumes 90–95, copyright © 1993–1998 by THE NATIONAL ACADEMY OF SCIENCES OF THE UNITED STATES OF AMERICA, all rights reserved; Volumes 1–89, copyright as a collective work only [author(s) retains copyright to individual articles]. *Requests for Permission*: Address requests to reproduce material published in Volumes 1–89 to the original author(s); address other requests to the Permissions Office of the PROCEEDINGS, 2101 Constitution Avenue, NW, Washington, DC 20418 USA, FAX 202-625-4749. Please cite the exact material to be reprinted and state specifically where it will be used. *Photocopies*: The journal is registered with the Copyright Clearance Center, 222 Rosewood Drive, Danvers, MA 01923 USA, FAX 978-750-4470. Authorization to photocopy items for the internal or personal use of specific clients is granted by THE NATIONAL ACADEMY OF SCIENCES provided that the copier pays to the Center the fee stated in the code on the first page of each article. *Microforms*: Contact University Microfilms Inc., P.O. Box 1346, Ann Arbor, MI 48106-1346 USA. This journal is printed on acid-free paper effective with Volume 84, Issue 1.

Subscriptions: Address subscription correspondence to the Circulation Office of the PROCEEDINGS, 2101 Constitution Avenue, NW, Washington, DC 20418 USA. Subscriptions are entered on a calendar-year basis only. The 1998 subscription rates for print only/online only/print plus online are as follows—in the U.S.: student, $90/$50/$110; postdoctoral, $125/$50/$150; personal, $165/$100/$195; institutional, $685/$615/$820—elsewhere (print by surface mail): student, $190/$50/$210; postdoctoral, $225/$50/$250; personal, $265/$100/$295; institutional, $785/$615/$920—elsewhere by expedited delivery at a surcharge of $320. Air mail rates available on request. *Exclusive Agent for Subscribers in Japan*: USACO Corporation, 13-12, Shimbashi, 1-Chome, Minato-ku, Tokyo 105 Japan. *Change of Address*: Notify the Circulation Office 6 weeks in advance and list the old and new addresses. The Academy is not responsible for nonreceipt of issues because of an improper address, unless a change of address is on file. *Claims*: Requests for replacement copies will not be honored more than 60 days after the issue date for domestic subscribers and not more than 90 days after the issue date for foreign subscribers. Claims will not be honored for more than 2 issues per calendar year for the same subscriber. *Single Copies*: $30 per issue in the U.S., $40 elsewhere. *Canadian GST*: Registration Number R-133130880.

Advertising: Contact FASEB AdNet, 9650 Rockville Pike, Bethesda, MD 20814-3998 USA. Phone 800-43-FASEB ×7103 or 301-530-7103, FAX 301-571-0683.

Postmaster: Send address changes to PROCEEDINGS OF THE NATIONAL ACADEMY OF SCIENCES, 2101 Constitution Avenue, NW, Washington, DC 20418 USA. Periodicals postage paid at Washington, DC, and additional mailing offices. PRINTED IN THE USA

PROCEEDINGS OF THE NATIONAL ACADEMY OF SCIENCES is also available online at http://www.pnas.org.

Cover photograph: Pasteur with microscope and books, saluting Asclepius, the Greek god of medicine: Panel from the bronze doors at the National Academy of Sciences.

PROCEEDINGS
OF THE
NATIONAL ACADEMY OF SCIENCES
OF THE UNITED STATES OF AMERICA

April 28, 1998 | Volume 95, Number 9 | pp. 4789–5420

Table of Contents

Commentaries

Plant parasitic nematodes: Digesting a page from the microbe book — 4789–4790
Noel T. Keen and Philip A. Roberts

HLA class I specificity for natural killer cell receptor CD94NKG2A: Two for one in more ways than one — 4791–4794
Wayne M. Yokoyama

Dynamics and function of proteins: The search for general concepts — 4795–4797
Hans Frauenfelder and Ben McMahon

From the Academy

List of New Members — 4798–4799

Physical Sciences

APPLIED MATHEMATICS

Line spectral analysis for harmonizable processes — 4800–4803
Keh-Shin Lii and Murray Rosenblatt

ASTRONOMY

Cosmological implications of a large complete quasar sample — 4804–4807
I. E. Segal and J. F. Nicoll

CHEMISTRY

Second-order correction to the Bigeleisen–Mayer equation due to the nuclear field shift — 4808–4809
Jacob Bigeleisen

Chemical requirements for inhibition of gap junction communication by the biologically active lipid oleamide — 4810–4815
Dale L. Boger, Jean E. Patterson, Xiaojun Guan, Benjamin F. Cravatt, Richard A. Lerner, and Norton B. Gilula

ENGINEERING

Engineering analysis of biological variables: An example of blood pressure over 1 day — 4816–4821
Wei Huang, Zheng Shen, Norden E. Huang, and Yuan Cheng Fung

GEOPHYSICS

The helium paradoxes — 4822–4827
Don L. Anderson

MATHEMATICS

On Calderón's conjecture for the bilinear Hilbert transform — 4828–4830
Michael T. Lacey and Christoph M. Thiele

Corteva Exhibit 2053 - Page 3 of 14
Bayer v. Corteva - IPR2023-01037

Contents

Biological Sciences

APPLIED BIOLOGICAL SCIENCES

Structure of the catalytic domain of avian sarcoma virus integrase with a bound HIV-1 integrase-targeted inhibitor — 4831–4836
Jacek Lubkowski, Fan Yang, Jerry Alexandratos, Alexander Wlodawer, He Zhao, Terrence R. Burke, Jr., Nouri Neamati, Yves Pommier, George Merkel, and Anna Marie Skalka

Highly resolved chemical imaging of living cells by using synchrotron infrared microspectrometry — 4837–4840
Nadège Jamin, Paul Dumas, Janine Moncuit, Wolf-Herman Fridman, Jean-Luc Teillaud, G. Lawrence Carr, and Gwyn P. Williams

Regulation of the zinc transporter ZnT-1 by dietary zinc — 4841–4846
Robert J. McMahon and Robert J. Cousins

BIOCHEMISTRY

Crystal structure of troponin C in complex with troponin I fragment at 2.3-Å resolution — 4847–4852
Dmitry G. Vassylyev, Soichi Takeda, Soichi Wakatsuki, Kayo Maeda, and Yuichiro Maéda

A primitive pathway of porphyrin biosynthesis and enzymology in *Desulfovibrio vulgaris* — 4853–4858
Tetsuo Ishida, Ling Yu, Hideo Akutsu, Kiyoshi Ozawa, Shosuke Kawanishi, Akira Seto, Toshiro Inubushi, and Seiyo Sano

Leukotriene D_4 and cystinyl-bis-glycine metabolism in membrane-bound dipeptidase-deficient mice — 4859–4863
Geetha M. Habib, Zheng-Zheng Shi, Allan A. Cuevas, Qiuxia Guo, Martin M. Matzuk, and Michael W. Lieberman

Regulation of a nuclear export signal by an adjacent inhibitory sequence: The effector domain of the influenza virus NS1 protein — 4864–4869
Yongzhong Li, Yoshihiko Yamakita, and Robert M. Krug

Experimental support for a β-propeller domain in integrin α-subunits and a calcium binding site on its lower surface — 4870–4875
Claus Oxvig and Timothy A. Springer

Crystal structures of two tropinone reductases: Different reaction stereospecificities in the same protein fold — 4876–4881
Keiji Nakajima, Atsuko Yamashita, Hiroyuki Akama, Toru Nakatsu, Hiroaki Kato, Takashi Hashimoto, Jun'ichi Oda, and Yasuyuki Yamada

Protein-bound acrolein: Potential markers for oxidative stress — 4882–4887
Koji Uchida, Masamichi Kanematsu, Kensuke Sakai, Tsukasa Matsuda, Nobutaka Hattori, Yoshikuni Mizuno, Daisuke Suzuki, Toshio Miyata, Noriko Noguchi, Etsuo Niki, and Toshihiko Osawa

Mechanism of platelet inhibition by nitric oxide: *In vivo* phosphorylation of thromboxane receptor by cyclic GMP-dependent protein kinase — 4888–4893
Guang-Rong Wang, Yan Zhu, Perry V. Halushka, Thomas M. Lincoln, and Michael E. Mendelsohn

Epstein–Barr virus growth-transformed cells are converted to malignancy following transfection of a 1.3-kb CATR1 antisense construct independent of a change in the level of *c-myc* expression followed by a 8;14 chromosomal translocation — 4894–4899
Dawei Li, Xiao Li Sun, Bruce Casto, Jin Fang, Karl Theil, Ronald Glaser, and George Milo

Escherichia coli rho factor induces release of yeast RNA polymerase II but not polymerase I or III — 4900–4905
Walter H. Lang, Terry Platt, and Ronald H. Reeder

Endogenous cellulases in animals: Isolation of β-1,4-endoglucanase genes from two species of plant-parasitic cyst nematodes — 4906–4911
Geert Smant, Jack P. W. G. Stokkermans, Yitang Yan, Jan M. de Boer, Thomas J. Baum, Xiaohong Wang, Richard S. Hussey, Fred J. Gommers, Bernard Henrissat, Eric L. Davis, Johannes Helder, Arjen Schots, and Jaap Bakker

The *Rhizobium meliloti* ExoK and ExsH glycanases specifically depolymerize nascent succinoglycan chains — 4912–4917
Gregory M. York and Graham C. Walker

Acetylation at Lys-92 enhances signaling by the chemotaxis response regulator protein CheY — 4918–4923
Ranjani Ramakrishnan, Martin Schuster, and Robert B. Bourret

Iron-dependent oxidation, ubiquitination, and degradation of iron regulatory protein 2: Implications for degradation of oxidized proteins — 4924–4928
Kazuhiro Iwai, Steven K. Drake, Nancy B. Wehr, Allan M. Weissman, Timothy LaVaute, Nagahiro Minato, Richard D. Klausner, Rodney L. Levine, and Tracey A. Rouault

Stable alteration of pre-mRNA splicing patterns by modified U7 small nuclear RNAs — 4929–4934
Linda Gorman, Daniel Suter, Victoria Emerick, Daniel Schümperli, and Ryszard Kole

Specificity in cholesterol regulation of gene expression by coevolution of sterol regulatory DNA element and its binding protein — 4935–4940
Jyoti N. Athanikar and Timothy F. Osborne

Mapping of the ligand-selective domain of the *Xenopus laevis* corticotropin-releasing factor receptor 1: Implications for the ligand-binding site — 4941–4946
Frank M. Dautzenberg, Sandra Wille, Ragna Lohmann, and Joachim Spiess

Perturbation of nucleosome core structure by the SWI/SNF complex persists after its detachment, enhancing subsequent transcription factor binding — 4947–4952
Jacques Côté, Craig L. Peterson, and Jerry L. Workman

A stationary phase protein in *Escherichia coli* with binding activity to the major σ subunit of RNA polymerase — 4953–4958
Miki Jishage and Akira Ishihama

Evidence that HetR protein is an unusual serine-type protease — 4959–4963
Ruanbao Zhou, Xingcheng Wei, Nan Jiang, Huiguang Li, Yuqing Dong, Kuo-L. Hsi, and Jindong Zhao

Corteva Exhibit 2053 - Page 4 of 14
Bayer v. Corteva - IPR2023-01037

Contents

BIOPHYSICS

Phospholipid composition of the mammalian red cell membrane can be rationalized by a superlattice model — 4964–4969
J. A. Virtanen, K. H. Cheng, and P. Somerharju

Dynamics of different functional parts of bacteriorhodopsin: H-^{2}H labeling and neutron scattering — 4970–4975
Valérie Réat, Heiko Patzelt, Michel Ferrand, Claude Pfister, Dieter Oesterhelt, and Giuseppe Zaccai

How evolution makes proteins fold quickly — 4976–4981
Leonid A. Mirny, Victor I. Abkevich, and Eugene I. Shakhnovich

The sequences of small proteins are not extensively optimized for rapid folding by natural selection — 4982–4986
David E. Kim, Hongdi Gu, and David Baker

Are protein folds atypical? — 4987–4990
Hao Li, Chao Tang, and Ned S. Wingreen

CELL BIOLOGY

Localization of nascent RNA and CREB binding protein with the PML-containing nuclear body — 4991–4996
Vickie J. LaMorte, Jacqueline A. Dyck, Robert L. Ochs, and Ronald M. Evans

Bax directly induces release of cytochrome *c* from isolated mitochondria — 4997–5002
Juliane M. Jürgensmeier, Zhihua Xie, Quinn Deveraux, Lisa Ellerby, Dale Bredesen, and John C. Reed

Transmembrane heme delivery systems — 5003–5008
Barry S. Goldman, David L. Beck, Elizabeth M. Monika, and Robert G. Kranz

Endothelial Ca^{2+} waves preferentially originate at specific loci in caveolin-rich cell edges — 5009–5014
Masashi Isshiki, Joji Ando, Risa Korenaga, Hiroshi Kogo, Toyoshi Fujimoto, Toshiro Fujita, and Akira Kamiya

Association of calcium channel α_{1S} and β_{1a} subunits is required for the targeting of β_{1a} but not of α_{1S} into skeletal muscle triads — 5015–5020
Birgit Neuhuber, Uli Gerster, Frank Döring, Hartmut Glossmann, Tsutomu Tanabe, and Bernhard E. Flucher

A distinct cyclin-dependent kinase-activating kinase of *Arabidopsis thaliana* — 5021–5026
Masaaki Umeda, Rishikesh P. Bhalerao, Jeff Schell, Hirofumi Uchimiya, and Csaba Koncz

A cytoplasmic protein, bystin, interacts with trophinin, tastin, and cytokeratin and may be involved in trophinin-mediated cell adhesion between trophoblast and endometrial epithelial cells — 5027–5032
Nao Suzuki, Jane Zara, Takaaki Sato, Edgar Ong, Nouna Bakhiet, Robert G. Oshima, Kellie L. Watson, and Michiko N. Fukuda

Targeted disruption of $p70^{s6k}$ defines its role in protein synthesis and rapamycin sensitivity — 5033–5038
Hideki Kawasome, Philip Papst, Saiphone Webb, Gordon M. Keller, Gary L. Johnson, Erwin W. Gelfand, and Naohiro Terada

Cellular memory: Neutrophil orientation reverses during temporally decreasing chemoattractant concentrations — 5039–5044
Eric Albrecht and Howard R. Petty

Macrophages resistant to endogenously generated nitric oxide-mediated apoptosis are hypersensitive to exogenously added nitric oxide donors: Dichotomous apoptotic response independent of caspase 3 and reversal by the mitogen-activated protein kinase kinase (MEK) inhibitor PD 098059 — 5045–5050
Susanne Mohr, Thomas S. McCormick, and Eduardo G. Lapetina

Activation of protein tyrosine kinase PYK2 by the m1 muscarinic acetylcholine receptor — 5051–5056
Jason S. Felsch, Teresa G. Cachero, and Ernest G. Peralta

Sequestration of the G protein $\beta\gamma$ subunit complex inhibits receptor-mediated endocytosis — 5057–5060
Hsin Chieh Lin, Joseph A. Duncan, Tohru Kozasa, and Alfred G. Gilman

Activation of apurinic/apyrimidinic endonuclease in human cells by reactive oxygen species and its correlation with their adaptive response to genotoxicity of free radicals — 5061–5066
Chilakamarti V. Ramana, Istvan Boldogh, Tadahide Izumi, and Sankar Mitra

DEVELOPMENTAL BIOLOGY

Solution structure of SpoIIAA, a phosphorylatable component of the system that regulates transcription factor σ^F of *Bacillus subtilis* — 5067–5071
Helena Kovacs, David Comfort, Matthew Lord, Iain D. Campbell, and Michael D. Yudkin

Rescue of *Caenorhabditis elegans* pharyngeal development by a vertebrate heart specification gene — 5072–5075
Christina Haun, Jonathan Alexander, Didier Y. Stainier, and Peter G. Okkema

A paracrine role for the epithelial progesterone receptor in mammary gland development — 5076–5081
Cathrin Brisken, Sissela Park, Tibor Vass, John P. Lydon, Bert W. O'Malley, and Robert A. Weinberg

Targeted disruption of fibroblast growth factor (FGF) receptor 2 suggests a role for FGF signaling in pregastrulation mammalian development — 5082–5087
Esther Arman, Rebecca Haffner-Krausz, Yali Chen, John K. Heath, and Peter Lonai

EVOLUTION

The role of robustness and changeability on the origin and evolution of genetic codes — 5088–5093
Tetsuya Maeshiro and Masayuki Kimura

Toward a resolution of the introns early/late debate: Only phase zero introns are correlated with the structure of ancient proteins — 5094–5099
Sandro J. de Souza, Manyuan Long, Robert J. Klein, Scott Roy, Shin Lin, and Walter Gilbert

Signaling among relatives. III. Talk is cheap — 5100–5105
Carl T. Bergstrom and Michael Lachmann

Corteva Exhibit 2053 - Page 5 of 14
Bayer v. Corteva - IPR2023-01037

Contents

Runaway ornament diversity caused by Fisherian sexual selection 5106–5111
Andrew Pomiankowski and Yoh Iwasa

Diploid hybrid speciation in *Penstemon* (Scrophulariaceae) 5112–5115
Andrea D. Wolfe, Qiu-Yun Xiang, and Susan R. Kephart

The hypoglossal canal and the origin of human vocal behavior 5417–5419
Richard F. Kay, Matt Cartmill, and Michelle Balow

GENETICS

Separation of killing and tumorigenic effects of an alkylating agent in mice defective in two of the DNA repair genes 5116–5120
Hisaya Kawate, Kunihiko Sakumi, Teruhisa Tsuzuki, Yoko Nakatsuru, Takatoshi Ishikawa, Seiichi Takahashi, Hiroshi Takano, Tetsuo Noda, and Mutsuo Sekiguchi

Modification of bacterial artificial chromosomes through Chi-stimulated homologous recombination and its application in zebrafish transgenesis 5121–5126
Jason R. Jessen, Anming Meng, Ramsay J. McFarlane, Barry H. Paw, Leonard I. Zon, Gerald R. Smith, and Shuo Lin

Tight clustering and hemizygosity of apomixis-linked molecular markers in *Pennisetum squamulatum* implies genetic control of apospory by a divergent locus that may have no allelic form in sexual genotypes 5127–5132
Peggy Ozias-Akins, Dominique Roche, and Wayne W. Hanna

Reactivation of *XIST* in normal fibroblasts and a somatic cell hybrid: Abnormal localization of XIST RNA in hybrid cells 5133–5138
R. Scott Hansen, Theresa K. Canfield, Ann M. Stanek, Elizabeth A. Keitges, and Stanley M. Gartler

A role for Pak protein kinases in Schwann cell transformation 5139–5144
Yi Tang, Sunil Marwaha, J. Lynn Rutkowski, Gihan I. Tennekoon, Peter C. Phillips, and Jeffrey Field

Evolution of rhizobia by acquisition of a 500-kb symbiosis island that integrates into a phe-tRNA gene 5145–5149
John T. Sullivan and Clive W. Ronson

Monosomy of a specific chromosome determines L-sorbose utilization: A novel regulatory mechanism in *Candida albicans* 5150–5155
Guilhem Janbon, Fred Sherman, and Elena Rustchenko

ARC, an inhibitor of apoptosis expressed in skeletal muscle and heart that interacts selectively with caspases 5156–5160
Takeyoshi Koseki, Naohiro Inohara, Shu Chen, and Gabriel Núñez

Mutation of the Sry-related *Sox10* gene in *Dominant megacolon*, a mouse model for human Hirschsprung disease 5161–5165
Beate Herbarth, Veronique Pingault, Nadege Bondurand, Kirsten Kuhlbrodt, Irm Hermans-Borgmeyer, Aldamaria Puliti, Nicole Lemort, Michel Goossens, and Michael Wegner

An oncogenic form of p53 confers a dominant, gain-of-function phenotype that disrupts spindle checkpoint control 5166–5171
Antonio Gualberto, Kenneth Aldape, Krystyna Kozakiewicz, and Thea D. Tlsty

Homology-directed repair is a major double-strand break repair pathway in mammalian cells 5172–5177
Feng Liang, Mingguang Han, Peter J. Romanienko, and Maria Jasin

Putative pheromone receptors related to the Ca^{2+}-sensing receptor in *Fugu* 5178–5181
Takayuki Naito, Yutaka Saito, Jun Yamamoto, Yuko Nozaki, Keiko Tomura, Masaaki Hazama, Shigetada Nakanishi, and Sydney Brenner

Transposition of the *mariner* element from *Drosophila mauritiana* in zebrafish 5182–5186
James M. Fadool, Daniel L. Hartl, and John E. Dowling

A genetic system based on split-ubiquitin for the analysis of interactions between membrane proteins *in vivo* 5187–5192
Igor Stagljar, Chantal Korostensky, Nils Johnsson, and Stephan te Heesen

IMMUNOLOGY

Predicting amino acid sequences of the antibody human V_H chains from its first several residues 5193–5198
Boris A. Galitsky, Israel M. Gelfand, and Alexander E. Kister

HLA-E is a major ligand for the natural killer inhibitory receptor CD94/NKG2A 5199–5204
Ni Lee, Manuel Llano, Marta Carretero, Akiko Ishitani, Francisco Navarro, Miguel López-Botet, and Daniel E. Geraghty

CD40 ligand (CD154) stimulation of macrophages to produce HIV-1-suppressive β-chemokines 5205–5210
Richard S. Kornbluth, Kristin Kee, and Douglas D. Richman

Identification of a meiosis-specific protein as a member of the class of cancer/testis antigens 5211–5216
Özlem Türeci, Ugur Sahin, Carsten Zwick, Michael Kosłowski, Gerhard Seitz, and Michael Pfreundschuh

On defining the rules for interactions between the T cell receptor and its ligand: A critical role for a specific amino acid residue of the T cell receptor β chain 5217–5222
Fuming Wang, Toshiro Ono, Alexis M. Kalergis, Weijia Zhang, Teresa P. DiLorenzo, Kap Lim, and Stanley G. Nathenson

Generation of CD8 suppressor factor and β chemokines, induced by xenogeneic immunization, in the prevention of simian immunodeficiency virus infection in macaques 5223–5228
Yufei Wang, Louisa Tao, Elaine Mitchell, Willy M. J. M. Bogers, Carl Doyle, Christopher A. Bravery, Lesley A. Bergmeier, Charles G. Kelly, Jonathan L. Heeney, and Thomas Lehner

Bacteria-induced neo-biosynthesis, stabilization, and surface expression of functional class I molecules in mouse dendritic cells 5229–5234
Maria Rescigno, Stefania Citterio, Clotilde Thèry, Michael Rittig, Donata Medaglini, Gianni Pozzi, Sebastian Amigorena, and Paola Ricciardi-Castagnoli

Corteva Exhibit 2053 - Page 6 of 14
Bayer v. Corteva - IPR2023-01037

Contents

Differences in the level of expression of class I major histocompatibility complex proteins on thymic epithelial and dendritic cells influence the decision of immature thymocytes between positive and negative selection — 5235–5240
Joseph R. Delaney, Yuri Sykulev, Herman N. Eisen, and Susumu Tonegawa

MEDICAL SCIENCES

The CCR5 receptor acts as an alloantigen in CCR5Δ32 homozygous individuals: Identification of chemokine- and HIV-1-blocking human antibodies — 5241–5245
Henrik J. Ditzel, Mette M. Rosenkilde, Peter Garred, Meng Wang, Klaus Koefoed, Court Pedersen, Dennis R. Burton, and Thue W. Schwartz

Inactivation of the tumor suppressor PTEN/MMAC1 in advanced human prostate cancer through loss of expression — 5246–5250
Young E. Whang, Xinyi Wu, Hiroyoshi Suzuki, Robert E. Reiter, Chris Tran, Robert L. Vessella, Jonathan W. Said, William B. Isaacs, and Charles L. Sawyers

Modulation of ventricular function through gene transfer *in vivo* — 5251–5256
Roger J. Hajjar, Ulrich Schmidt, Takashi Matsui, J. Luis Guerrero, Kyung-Han Lee, Judith K. Gwathmey, G. William Dec, Marc J. Semigran, and Anthony Rosenzweig

Autologously up-regulated Fc receptor expression and action in airway smooth muscle mediates its altered responsiveness in the atopic asthmatic sensitized state — 5257–5262
H. Hakonarson and M. M. Grunstein

Lipophilic siderophores of *Mycobacterium tuberculosis* prevent cardiac reperfusion injury — 5263–5268
Lawrence D. Horwitz, Nancy A. Sherman, Yinong Kong, Adrian W. Pike, Jovana Gobin, Paul V. Fennessey, and Marcus A. Horwitz

Targeted expression of a multifunctional chimeric neurotrophin in the lesioned sciatic nerve accelerates regeneration of sensory and motor axons — 5269–5274
Hiroshi Funakoshi, Mårten Risling, Thomas Carlstedt, Urban Lendahl, Tõnis Timmusk, Madis Metsis, Yuji Yamamoto, and Carlos F. Ibáñez

Increased skin tumorigenesis in mice lacking pi class glutathione *S*-transferases — 5275–5280
Colin J. Henderson, Austin G. Smith, Jan Ure, Ken Brown, E. Jane Bacon, and C. Roland Wolf

HIV transcriptional activation by the accessory protein, VPR, is mediated by the p300 co-activator — 5281–5286
Lisa K. Felzien, Clive Woffendin, Michael O. Hottiger, Ramu A. Subbramanian, Eric A. Cohen, and Gary J. Nabel

The BRC repeats in BRCA2 are critical for RAD51 binding and resistance to methyl methanesulfonate treatment — 5287–5292
Phang-Lang Chen, Chi-Fen Chen, Yumay Chen, Jun Xiao, Z. Dave Sharp, and Wen-Hwa Lee

MICROBIOLOGY

Agrobacterium transcriptional regulator Ros is a prokaryotic zinc finger protein that regulates the plant oncogene *ipt* — 5293–5298
Alan Y. Chou, John Archdeacon, and Clarence I. Kado

Mycobacterium bovis bacille Calmette–Guérin strains secreting listeriolysin of *Listeria monocytogenes* — 5299–5304
Jürgen Hess, Diana Miko, André Catic, Vera Lehmensiek, David G. Russell, and Stefan H. E. Kaufmann

DNA strand separation during activation of a developmental promoter by the *Bacillus subtilis* response regulator Spo0A — 5305–5310
Dean A. Rowe-Magnus and George B. Spiegelman

Down-regulation of *Leishmania donovani* trypanothione reductase by heterologous expression of a trans-dominant mutant homologue: Effect on parasite intracellular survival — 5311–5316
Jorge Tovar, Mark L. Cunningham, Aden C. Smith, Simon L. Croft, and Alan H. Fairlamb

Antibacterial agents that inhibit two-component signal transduction systems — 5317–5322
J. F. Barrett, R. M. Goldschmidt, L. E. Lawrence, B. Foleno, R. Chen, J. P. Demers, S. Johnson, R. Kanojia, J. Fernandez, J. Bernstein, L. Licata, A. Donetz, S. Huang, D. J. Hlasta, M. J. Macielag, K. Ohemeng, R. Frechette, M. B. Frosco, D. H. Klaubert, J. M. Whiteley, L. Wang, and J. A. Hoch

NEUROBIOLOGY

Differential signaling via the same axon of neocortical pyramidal neurons — 5323–5328
Henry Markram, Yun Wang, and Misha Tsodyks

Regulation of thalamic neurite outgrowth by the Eph ligand ephrin-A5: Implications in the development of thalamocortical projections — 5329–5334
Pan-Pan Gao, Yong Yue, Jian-Hua Zhang, Douglas Pat Cerretti, Pat Levitt, and Renping Zhou

Maternal care during infancy regulates the development of neural systems mediating the expression of fearfulness in the rat — 5335–5340
Christian Caldji, Beth Tannenbaum, Shakti Sharma, Darlene Francis, Paul M. Plotsky, and Michael J. Meaney

A subclass of prefrontal γ-aminobutyric acid axon terminals are selectively altered in schizophrenia — 5341–5346
Tsung-Ung Woo, Richard E. Whitehead, Darlene S. Melchitzky, and David A. Lewis

Reinnervation of cross-regenerated gustatory nerve fibers into amiloride-sensitive and amiloride-insensitive taste receptor cells — 5347–5350
Yuzo Ninomiya

High expression levels in cones of RGS9, the predominant GTPase accelerating protein of rods — 5351–5356
Christopher W. Cowan, Robert N. Fariss, Izabela Sokal, Krzysztof Palczewski, and Theodore G. Wensel

Corteva Exhibit 2053 - Page 7 of 14
Bayer v. Corteva - IPR2023-01037

Contents

PHARMACOLOGY

Effect of intravenous infusions of 12-O-tetradecanoylphorbol-13-acetate (TPA) in patients with myelocytic leukemia: Preliminary studies on therapeutic efficacy and toxicity 5357–5361
Zheng Tao Han, Xiao Xiu Zhu, Ru Yu Yang, Jun Zhong Sun, Guo Fang Tian, Xin Jian Liu, Guo Shun Cao, Harold L. Newmark, Allan H. Conney, and Richard L. Chang

12-O-Tetradecanoylphorbol-13-acetate (TPA)-induced increase in depressed white blood cell counts in patients treated with cytotoxic cancer chemotherapeutic drugs 5362–5365
Zheng Tao Han, Yun Ke Tong, Lin Min He, Yang Zhang, Jun Zhong Sun, Tian Yi Wang, Hong Zhang, Ya Ling Cui, Harold L. Newmark, Allan H. Conney, and Richard L. Chang

Nerve growth factor abrogates the tumorigenicity of human small cell lung cancer cell lines 5366–5371
Cristina Missale, Agnese Codignola, Sandra Sigala, Alessandra Finardi, Marcelo Paez-Pereda, Emanuele Sher, and PierFranco Spano

PHYSIOLOGY

Targeted inactivation of *Npt2* in mice leads to severe renal phosphate wasting, hypercalciuria, and skeletal abnormalities 5372–5377
Laurent Beck, Andrew C. Karaplis, Norio Amizuka, A. Stacy Hewson, Hidehiro Ozawa, and Harriet S. Tenenhouse

Migrating transformed MDCK cells are able to structurally polarize a voltage-activated K^+ channel 5378–5382
J. Reinhardt, N. Golenhofen, O. Pongs, H. Oberleithner, and A. Schwab

Phosphorylation of a twitchin-related protein controls catch and calcium sensitivity of force production in invertebrate smooth muscle 5383–5388
Marion J. Siegman, Daisuke Funabara, Shigeharu Kinoshita, Shugo Watabe, David J. Hartshorne, and Thomas M. Butler

Expression of the Na^+/Ca^{2+} exchanger emerges in hepatic stellate cells after activation in association with liver fibrosis 5389–5394
Toshio Nakamura, Shigeki Arii, Kazunobu Monden, Masaharu Furutani, Yoshihisa Takeda, Masayuki Imamura, Makoto Tominaga, and Yasunobu Okada

Cloning and characterization of a potassium-coupled amino acid transporter 5395–5400
Michela Castagna, Chairat Shayakul, Davide Trotti, V. Franca Sacchi, William R. Harvey, and Matthias A. Hediger

PLANT BIOLOGY

Association of the *Arabidopsis* CTR1 Raf-like kinase with the ETR1 and ERS ethylene receptors 5401–5406
Karen L. Clark, Paul B. Larsen, Xiaoxia Wang, and Caren Chang

Compartmentalized expression of two structurally and functionally distinct 4-coumarate:CoA ligase genes in aspen (*Populus tremuloides*) 5407–5412
Wen-Jing Hu, Akiyoshi Kawaoka, Chung-Jui Tsai, Jrhau Lung, Keishi Osakabe, Hiroyasu Ebinuma, and Vincent L. Chiang

PSYCHOLOGY

Visual memory-deficit amnesia: A distinct amnesic presentation and etiology 5413–5416
David C. Rubin and Daniel L. Greenberg

Social Sciences

ANTHROPOLOGY

The hypoglossal canal and the origin of human vocal behavior 5417–5419
Richard F. Kay, Matt Cartmill, and Michelle Balow

CORRECTIONS

BIOCHEMISTRY

Cloning of the cDNA for the TATA-binding protein-associated factor$_{II}$170 subunit of transcription factor B-TFIID reveals homology to global transcription regulators in yeast and *Drosophila* 5420
Jan A. van der Knaap, Jan Willem Borst, Peter C. van der Vliet, Reiner Gentz, and H. Th. Marc Timmers

NEUROBIOLOGY

Elevated free nitrotyrosine levels, but not protein-bound nitrotyrosine or hydroxyl radicals, throughout amyotrophic lateral sclerosis (ALS)-like disease implicate tyrosine nitration as an aberrant *in vivo* property of one familial ALS-linked superoxide dismutase 1 mutant 5420
L. I. Bruijn, M. F. Beal, M. W. Becher, J. B. Schulz, P. C. Wong, D. L. Price, and D. W. Cleveland

AUTHOR INDEX xi–xiii

INFORMATION FOR AUTHORS xiv–xvi

SIZING WORKSHEET xvii

SUBSCRIPTION FORM xviii

COPYRIGHT ASSIGNMENT FORM xix

CLASSIFIED ADVERTISEMENTS xx–xxii

Corteva Exhibit 2053 - Page 8 of 14
Bayer v. Corteva - IPR2023-01037

This material may be protected by Copyright law (Title 17 U.S. Code)

Proc. Natl. Acad. Sci. USA
Vol. 95, pp. 4876–4881, April 1998
Biochemistry

Crystal structures of two tropinone reductases: Different reaction stereospecificities in the same protein fold

KEIJI NAKAJIMA*†, ATSUKO YAMASHITA‡, HIROYUKI AKAMA*, TORU NAKATSU‡, HIROAKI KATO‡, TAKASHI HASHIMOTO*, JUN'ICHI ODA‡, AND YASUYUKI YAMADA*

*Graduate School of Biological Sciences, Nara Institute of Science and Technology, Ikoma, Nara 630-0101, Japan; and ‡Institute for Chemical Research, Kyoto University, Uji, Kyoto 611-0011, Japan

Communicated by Rodney B. Croteau, Washington State University, Pullman, WA, February 18, 1998 (received for review December 15, 1997)

ABSTRACT **A pair of tropinone reductases (TRs) share 64% of the same amino acid residues and belong to the short-chain dehydrogenase/reductase family. In the synthesis of tropane alkaloids in several medicinal plants, the TRs reduce a carbonyl group of an alkaloid intermediate, tropinone, to hydroxy groups with different diastereomeric configurations. To clarify the structural basis for their different reaction stereospecificities, we determined the crystal structures of the two enzymes at 2.4- and 2.3-Å resolutions. The overall folding of the two enzymes was almost identical. The conservation was not confined within the core domains that are conserved within the protein family but extended outside the core domain where each family member has its characteristic structure. The binding sites for the cofactor and the positions of the active site residues were well conserved between the two TRs. The substrate binding site was composed mostly of hydrophobic amino acids in both TRs, but the presence of different charged residues conferred different electrostatic environments on the two enzymes. A modeling study indicated that these charged residues play a major role in controlling the binding orientation of tropinone within the substrate binding site, thereby determining the stereospecificity of the reaction product. The results obtained herein raise the possibility that in certain cases different stereospecificities can be acquired in enzymes by changing a few amino acid residues within substrate binding sites.**

Two tropinone reductases (TRs) constitute a branching point in the biosynthetic pathway of tropane alkaloids, which include such medicinally important compounds as hyoscyamine (atropine) and cocaine. TRs catalyze NADPH-dependent reductions of the 3-carbonyl group of their common substrate, tropinone, to hydroxy groups with different diastereomeric configurations: TR-I (EC 1.1.1.206) produces tropine (3α-hydroxytropane), and TR-II (EC 1.1.1.236) produces pseudotropine (ψ-tropine, 3β-hydroxytropane) (Fig. 1). All the tropane alkaloid-producing plant species so far examined have two TR activities (1), and their amino acid sequences are known from two species, *Datura stramonium* (2) and *Hyoscyamus niger* (ref. 3 and unpublished results). In both these species, TR-I and TR-II share 64% of the same amino acid residues and, therefore, are thought to have diverged relatively recently from a common ancestral protein. The amino acid sequences of these TRs also have the characteristic motifs of enzymes that belong to the short-chain dehydrogenase/reductase (SDR) family (4).

The most intriguing question concerning the two TRs is what protein structures enable the enzymes to produce different stereoisomers from the same substrate tropinone. Analyses of chimeric TR enzymes suggest that the C-terminal polypeptide spanning 120 amino acid residues constitutes most of the substrate binding site and that the distinct stereospecificities of the TR reactions are conferred by their structural differences (5). Within this 120-residue region, 53 residues differ between TR-I and TR-II (5). This degree of nonhomology may be sufficient to alter the protein folding in this region and to provide different structural motifs at the substrate binding sites. Conversely, only a small number of the amino acid residues that differ between TR-I and TR-II may actually participate in determining the stereospecificities, and the overall foldings of the two enzymes may not be as different as predicted from their primary structures. To determine which of the two possibilities is true for the TRs, we determined the crystal structures of the TRs from *D. stramonium*. The structures revealed a simple evolutionary process adopted by the TRs to acquire their different stereospecificities.

MATERIALS AND METHODS

Protein Preparation. The *D. stramonium* TR-I and TR-II cDNAs were subcloned from pTR1EN and pTR2EN (5) into pET-21d (Novagen) to give pETTR1 and pETTR2, respectively. TR proteins were induced in *Escherichia coli* BL21(DE3) by 0.1 mM isopropyl β-D-thiogalactoside (TR-I, 37°C for 3 hr; TR-II, 25°C for 16 hr). Bacteria were lysed in 100 mM potassium phosphate (pH 7.0) containing 3 mM DTT, 0.1% Triton X-100, and lysozyme (10 μg/ml), by three rounds of a freeze–thaw cycle followed by sonication. The lysate was centrifuged and the supernatant was fractionated with ammonium sulfate (45–75% saturation). TR-I was purified by a series of chromatographies on butyl-Sepharose (Pharmacia), Red-Toyopearl (Toso, Tokyo), phenyl-Superose (Pharmacia), and Mono Q (Pharmacia). Purification of TR-II was done similarly by using three chromatographic steps (A.Y., K.N., H.K., T.H., Y.Y., and J.O., unpublished results).

Crystallization. TR-I was crystallized as a complex with $NADP^+$ by the hanging-drop vapor diffusion method at 20°C. Hanging drops (4–10 μl) were prepared by mixing equal volumes of the protein solution [TR-I (9 mg/ml)/5 mM Tris·HCl, pH 7.5/8 mM $NADP^+$/2 mM DTT] and the reservoir solution [50 mM sodium citrate, pH 4.4/16–20% (vol/vol) PEG 1000/0.18–0.20 M magnesium acetate]. Crystals grew to an average size of 0.8 × 0.5 × 0.2 mm. The TR-I crystal was found to belong to the $P2_12_12$ space group with cell dimensions of a = 55.7 Å, b = 122.7 Å, and c = 75.5 Å. TR-II was crystallized by hanging-drop vapor diffusion with 2-methyl-

The publication costs of this article were defrayed in part by page charge payment. This article must therefore be hereby marked "*advertisement*" in accordance with 18 U.S.C. §1734 solely to indicate this fact.

© 1998 by The National Academy of Sciences 0027-8424/98/954876-6$2.00/0
PNAS is available online at http://www.pnas.org.

Abbreviations: TR, tropinone reductase; SDR, short-chain dehydrogenase/reductase; LDH, lactate dehydrogenase.

Data deposition: The atomic coordinates and structure factors have been deposited in the Protein Data Bank, Biology Department, Brookhaven National Laboratory, Upton, NY 11973 (accession codes 1ae1 for TR-I and 2ae1 for TR-II).

†To whom reprint requests should be addressed. e-mail: k-nakaji@bs.aist-nara.ac.jp.

Corteva Exhibit 2053 - Page 9 of 14
Bayer v. Corteva - IPR2023-01037

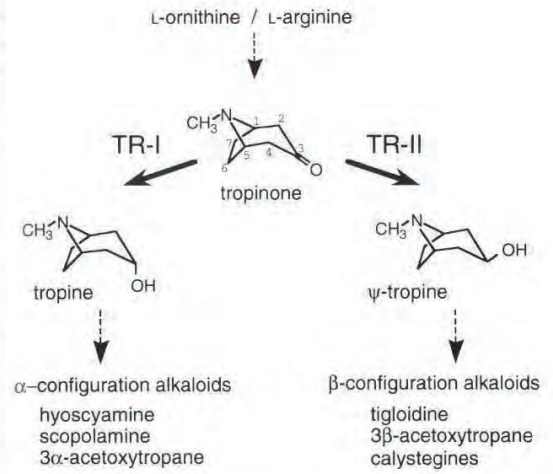

FIG. 1. Reactions catalyzed by TRs. TRs reduce the carbonyl group of a common substrate, tropinone, to hydroxy groups with different configurations. The reaction products tropine (3α-hydroxytropane) and ψ-tropine (3β-hydroxytropane) do not interconvert, rather they are further metabolized to various alkaloid products. Both enzymes require NADPH as the hydride donor. Carbon atoms of the tropane ring system are numbered in tropinone.

2,4-pentanediol used as a precipitating reagent (A.Y., K.N., H.K., T.H., Y.Y., and J.O., unpublished results). The TR-II crystals formed in the drop were grown further by a macroseeding technique. The crystal belonged to the $P4_22_12$ space group with cell dimensions of $a = b = 62.8$ Å and $c = 128.4$ Å.

Data Collection and Processing. All the diffraction data sets were collected on an R-AXIS IIc image plate area detector (Rigaku, Tokyo). The x-ray source was monochromatized CuK_α generated from a rotating anode, RU300 (Rigaku), operating at 40 kV and 100 mA. Diffraction data of the TR-I crystal were collected from a single crystal by taking 61 frames of 1.5°-oscillation photographs. For the TR-II crystal, the cryocrystallograhic technique was used to reduce the crystal damage caused by the x-ray (A.Y., K.N., H.K., T.H., Y.Y., and J.O., unpublished results). Data were merged and scaled by using the PROCESS program (Rigaku). Statistics on the data collection and reduction are given in Table 1.

Phase Calculation, Model Building, and Refinement. All the structure determination procedures were done separately for each TR. The initial phases were calculated by the isomorphous replacement method using heavy metal derivative crystals prepared by soaking the crystals in a solution containing a heavy metal reagent. Determination and refinement of the heavy atom parameters and the subsequent phase calculation and improvement were done with the PHASES software package (6). For TR-I, only one ethylmercurithiosalicylate-derivative crystal showed good replacement by heavy atoms. The initial phase of the TR-I crystal was, therefore, calculated by using the single isomorphous replacement with anomalous scattering method. For TR-II, data sets from two heavy atom derivative crystals [$KAu(CN)_2$ and $HgCl_2$] were used for multiple isomorphous replacement phase calculation. Anomalous differences measured in the same data sets were also included. For both TR crystals, the initial phase was improved by the solvent flattening protocol (7). Conditions used to prepare the heavy atom derivatives, and the data collection and phase calculation statistics are given in Table 1.

Model building and corrections were done with the TURBO-FRODO program (BioGraphics, Marseilles, France). Models were first constructed in the protein regions for which electron density was readily interpretable. These partial structure models were used to calculate the protein phase angles, which then were combined with the isomorphous replacement phase. A new electron density map, calculated from the combined phase, was used to construct or confirm the model in the region where the previous map gave only poor electron density. This cycle was repeated several times throughout the model-building step. For the TR-I crystal, in which a dimer represents an asymmetric unit, a noncrystallographic twofold axis was found and refined by using the X-PLOR (8) and PHASES program packages. The correlation coefficient at the refined noncrystallographic axis was 0.748 at 5.0 Å. For the TR-I model building, a model was first constructed for one subunit of the dimer, after which it was turned around the noncrystallographic axis. This model was then corrected according to electron density.

The models were refined by using X-PLOR and REFMAC in the CCP4 program suite (9). In the initial stages, the structural model was refined by the slow-cool protocol (10), followed by positional and overall B factor refinements. The $2F_o - F_c$ and $F_o - F_c$ electron density maps were calculated and used to rebuild the structure models. This refinement-correction step was repeated many times. After the R values had dropped about 25%, the group B factors were refined. $NADP^+$ was then modeled within the TR-I structure, and solvent molecules were included in both of the TR structures by using the program WATERHUNTER (11). In the later stages, the model was refined by positional and individual B factor refinements. Resolution of the TR-I model was extended to the limit of the native data set (2.4 Å). Refinement of TR-II was completed at 2.3 Å, because data in the higher resolution range was of low quality and affected the refinement process adversely. Stereochemical properties of the models were assessed by the PROCHECK

Table 1. Data collection statistics for native and derivative crystals

Crystal	Soaking conditions	Maximum resolution, Å	No. of reflections		Completeness, %	R_{merge}, %	R_{deri}, %	R_{ano}, %	No. of sites	Phasing power	
			Total	Unique						Isomorphous	Anomalous
TRI-1											
Native		2.4	65,888	19,708	94.8	4.34					
EMTS	1 mM, 3 hr	2.4	58,320	18,603	92.4	5.97	5.9	2.4	3	2.57	2.58
TR-II											
Native		2.0	103,356	14,339	81.8	8.74					
$KAu(CN)_2$	1 mM, 6 days	2.6	46,382	8,069	94.8	8.61	4.4	2.5	2	1.58	1.35
$HgCl_2$	0.1 mM, 8 hr	2.6	52,405	8,374	97.7	6.08	3.3	1.3*	2	1.48	1.19*

$R_{merge} = \Sigma_h\Sigma_i|I_{h,i} - \langle I_h\rangle|/\Sigma_h\Sigma_i I_{h,i}$, where $I_{h,i}$ is the intensity of reflection h in data set i and $\langle I_h\rangle$ is the mean intensity of reflection h in the replicated data. $R_{deri} = \Sigma||F_{PH}| - |F_P||/\Sigma(|F_{PH}| + |F_P|)$, where $|F_{PH}|$ and $|F_P|$, respectively, are the structure factor amplitude of the derivative and native crystals. $R_{ano} = \Sigma||F_{PH(+)}| - |F_{PH(-)}||/\Sigma(|F_{PH(+)}| + |F_{PH(-)}|)$, where $|F_{PH(+)}|$ and $|F_{PH(-)}|$ are the structure factor amplitude of a Friedel pair. Phasing power $= (\Sigma|F_H|^2/\Sigma(|F_{PHobs}| - |F_{PHcalc}|)^2]^{1/2}$, where $|F_H|$ is the calculated structure factor amplitude of the heavy atom structure and $|F_{PHobs}|$ and $|F_{PHcalc}|$, respectively, are the observed and calculated structure factor amplitudes of the derivative crystals.
*Anomalous difference phase calculation of the $HgCl_2$ derivative was done by using reflection data to 3.0-Å resolution.

Corteva Exhibit 2053 - Page 10 of 14
Bayer v. Corteva - IPR2023-01037

Table 2. Refinement statistics

	TR-I	TR-II
Resolution range, Å	10.0–2.4	10.0–2.3
Reflections used in refinement, no.	18,143	10,999
R factor		
Work set	0.155	0.205
Test set	0.248	0.306
Test set size, %	5	6
No. of atoms		
Protein	3,828	1,922
Cofactor	96	—
Water	98	103
rms deviation from ideal value (protein)		
Bond length, Å	0.008	0.008
Bond angle, degrees	0.97	1.33
Dihedral angle, degrees	24.73	23.37
Improper angle, degrees	1.72	1.10
Residues in most favored regions of Ramachandran plot, %	90.4	90.0
Average *B* factor, Å^2		
Main chain	17.22	30.17
Side chain	23.18	33.09
Cofactor	16.10	—
Solvent	26.99	36.44

R factor = $\Sigma\,(|F_o| - |F_c|)/\Sigma\,|F_o|$, where $|F_o|$ and $|F_c|$, respectively, are the observed and calculated structure factor amplitudes.

program (12). The model refinement statistics are given in Table 2.

RESULTS AND DISCUSSION

Conserved Overall Structures Ensuring a Common Catalytic Mechanism. The structural model of TR-I includes residues 16–205* and 219–273 of one subunit (tentatively designated, chain A) and residues 16–273 of the other (chain B), as well as two NADP$^+$ and 98 water molecules per dimer. Electron densities corresponding to the residues 206–218 were visible only in chain B, most likely due to the stabilization of the crystal packing. Because the remaining parts of the two TR-I subunits are very similar (rms deviation = 0.25 Å), the structure of chain B is considered hereafter to be representative of the two subunits. For the TR-II crystal in which the two subunits of the dimer were crystallographically identical, the model contains residues 2–194 and 202–260 of the subunit plus 103 water molecules. Although the addition of tropinone was indispensable for TR-II crystallization, no electron density that would account for bound tropinone was visible throughout the refinement process.

The structures of the TR-I and TR-II dimers are shown in Fig. 2*A*. The two structures are almost indistinguishable from each other in both subunit folding and their association in dimers. Conservation of the subunit structures between TR-I and TR-II was substantiated when the two structures were superimposed by the least squares method using all equivalent Cα positions (Fig. 2*B*, rms deviation = 0.78 Å). Both TR subunits consist of a core domain that includes most of the polypeptide and a small lobe that protrudes from the core (Fig. 2*B*). A deep cleft was recognized between the core domain and the small lobe (Fig. 2*B*), which is presumed to be the binding site for tropinone. The cleft of each subunit is composed exclusively of the polypeptide from a single subunit and is oriented toward the opposite ends of the dimer ellipsoid (Fig. 2*A*). In the center of the core domain is a seven-stranded parallel β-sheet, flanked on each side by three α-helices, which constitutes the "Rossmann fold" topology (15). This core structure is highly conserved among the SDR family members, despite relatively low residue identity between these enzymes (~30%) (4, 16). Hereafter, the secondary structural elements of the TR subunits are referred to in a manner similar to those commonly used for the SDR family (Figs. 2*B* and 3). The small lobes of the two TRs are also very similar to each other, although the structure of this region is highly variable among SDRs for which crystal structures are known. In TR-II, the polypeptide corresponding to αG$''$ is disordered and, therefore, could not be modeled.

TR-I protein was crystallized in the presence of NADP$^+$, and the bound cofactor molecules in the protein structure could be modeled unambiguously. As seen in Fig. 2*B*, NADP$^+$

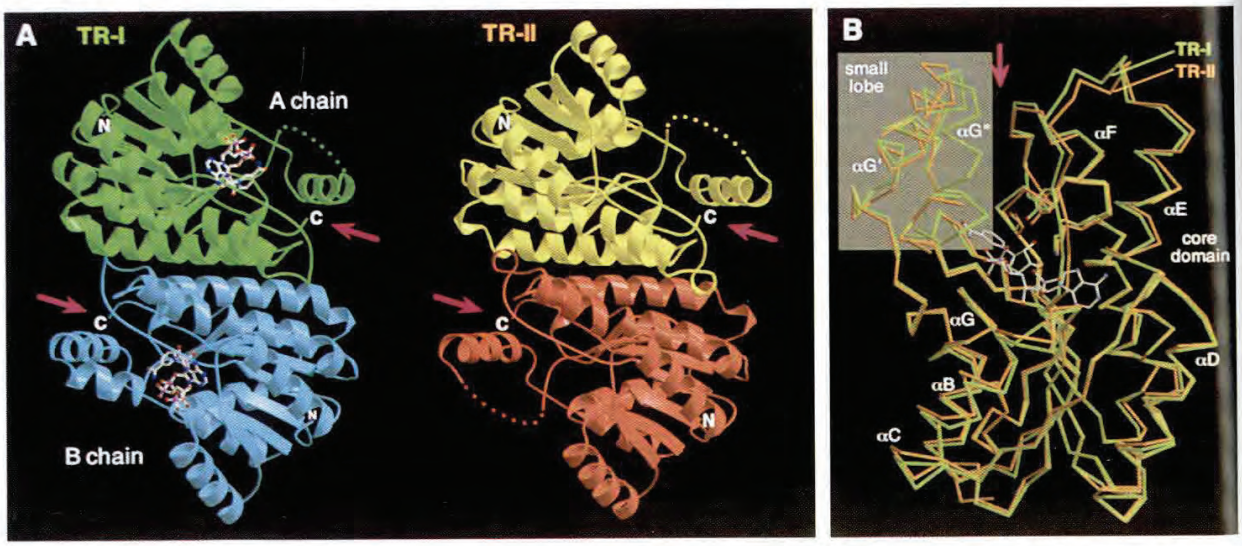

FIG. 2. (*A*) Structures of TR dimers. Subunits of TR-I (green and blue) and TR-II (yellow and red) are related, respectively, by a noncrystallographic and crystallographic twofold axis positioned at the center of each dimer and oriented perpendicular to the plane of the figure. NADP$^+$ bound in the TR-I subunits is shown by ball-and-stick models. Disordered regions in chain A of TR-I and both of the TR-II subunits are shown by dots. (*B*) Cα traces of TR-I (green) and TR-II (orange) subunits are superimposed by the program LSQKAB (9) using all possible Cα pairs. The binding position of NADP$^+$ in TR-I and the side chains of the three catalytic residues also are shown. The small lobes are shown in a gray background. Arrows indicate the clefts formed between the core domain and the small lobe (*A* and *B*). The figures were prepared by using the programs MOLSCRIPT (13) and RASTER3D (14).

Corteva Exhibit 2053 - Page 11 of 14
Bayer v. Corteva - IPR2023-01037

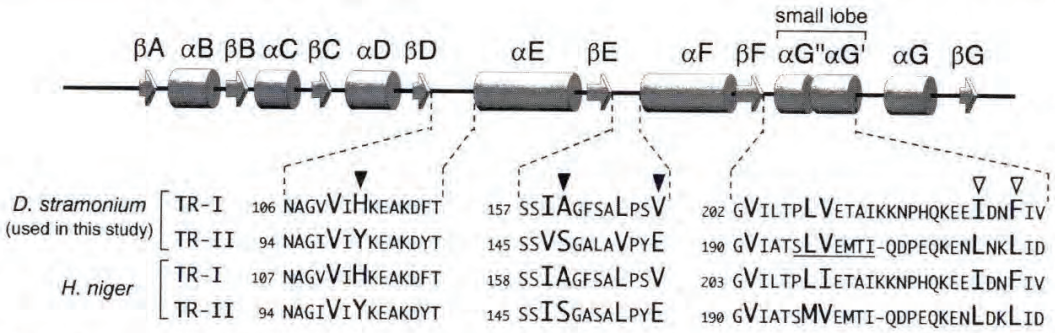

FIG. 3. Schematic representation of the secondary structural elements along the TR polypeptide. Amino acid sequence alignments are shown for the regions surrounding the putative tropinone binding residues. The sequences of the *H. niger* TRs are also shown for comparison. Amino acids predicted to be in contact with the tropinone substrate are shown in larger uppercase type, among which the positions with enzyme type-specific substitutions are indicated by arrowheads (solid arrowhead, substitution with polarity change; open arrowhead, substitution conserving hydrophobicity). The disordered TR-II polypeptide segment is underlined.

is located at the bottom of the cleft between the core domain and the small lobe. The carboxyamide group of the nicotinamide ring is anchored by the main-chain nitrogen and oxygen atoms of Ile-204 and the side-chain oxygen of Thr-206 (Fig. 4). This tight binding of the carboxyamide group to the protein directs the B-face of the nicotinamide ring toward the void of the cleft, consistent with the observed specificity for the pro-*S* hydride transfer of both TRs (1). In contrast to TR-I, well-ordered TR-II crystal was not obtained in the presence of the cofactor. The highly conserved architectures of the cofactor binding site of the two TRs, however, clearly indicates that the TR-II protein binds the cofactor in the same way as TR-I (Fig. 4). Although the conformations of the two TR-II side chains (Arg-19 and Arg-41) are very different from those of the corresponding TR-I residues (Lys-31 and Arg-53), the differences are considered to be caused by the binding of the cofactor to TR-I, because these two basic residues have been postulated to be of functional importance in the binding of NADPH preferably to NADH (17, 18).

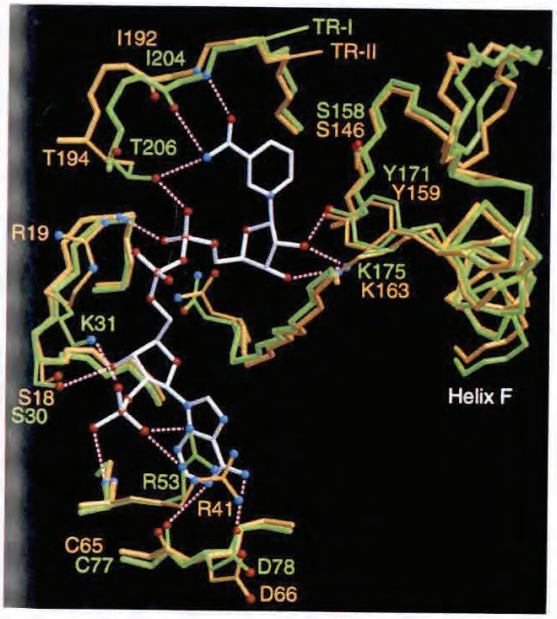

FIG. 4. Superimposition of the region encompassing the cofactor binding site and catalytic residues of TRs. The binding position of $NADP^+$ (bonds shown in white) was determined for TR-I. Bonds in the TR-I and TR-II proteins are shown in green and orange, respectively. For simplicity, only the protein side chains that directly interact with the cofactor atoms are shown. Possible hydrogen bonding interactions are indicated by dotted lines, although many other hydrogen bonding interactions through water molecules could be predicted from the structural model. Three catalytic residues (Ser, Tyr, Lys) are shown at the right. The figure was prepared by using the programs MOLSCRIPT (13) and RASTER3D (14).

The catalytic mechanism of SDRs has been predicted from the site-directed mutations and crystal structures of several enzymes (19–22). At present, the "Ser-Tyr-Lys catalytic triad" is considered to be important in SDR catalysis, whereby the side-chain oxygen of the Tyr functions as an acid–base catalyst for proton transfer. The three catalytic residues of TR-I and TR-II can also be superimposed very well, and the side-chain oxygen of the Tyr residue points toward the B-face of the cofactor nicotinamide ring (Fig. 4). This structural conservation clearly indicates that the reaction mechanism common to the SDR family also operates in both TR enzymes, namely, the concerted transfer of a hydride from NADPH and a proton from the Tyr residue to the 3-carbon and carbonyl oxygen atoms, respectively, of tropinone.

Modeling of Tropinone in Substrate Binding Sites. Concurrent conservation of the catalytic residues and the cofactor binding sites leaves only one explanation for the TR stereospecificities; tropinone should bind TR-I and TR-II in opposite orientations. To corroborate this rationale, we attempted crystallographic analyses of TR–cofactor–substrate ternary complexes. Soaking of the crystals in solutions containing the cofactor and tropinone under various conditions, however, did not add the required electron densities, probably due to inadequate crystal packing. While initiating an *ab initio* search for the crystallization conditions in the presence of the ligand molecules, we predicted from the present structural models the amino acid residues that would play important roles in orienting tropinone.

When the molecular surface of each TR with $NADP^+$ bound at its binding site was constructed based on the van der Waals radii of the protein and cofactor atoms, an empty space was found at the predicted tropinone binding site, i.e., the cleft between the core domain and small lobe (Fig. 5 *A* and *B*). For each TR, binding of tropinone was modeled in this space, so that its orientation and position would allow the production of the correct stereoisomer via the transfer of the pro-*S* hydride of NADPH and the proton of the Tyr residue from the proper sides of the bound tropinone.

The bound tropinone was predicted to contact about 10 amino acids in both TRs (Fig. 5 *C* and *D*). These residues are located either at the two loops in the core domain or in the two α-helices that constitute the small lobe (Fig. 3). The positive charge on the TR-I surface (Fig. 5*A*) is due to His-112, which in TR-II is replaced with Tyr-100, a polar but not basic residue. The negative charge on the TR-II surface (Fig. 5*B*) is gener-

Corteva Exhibit 2053 - Page 12 of 14
Bayer v. Corteva - IPR2023-01037

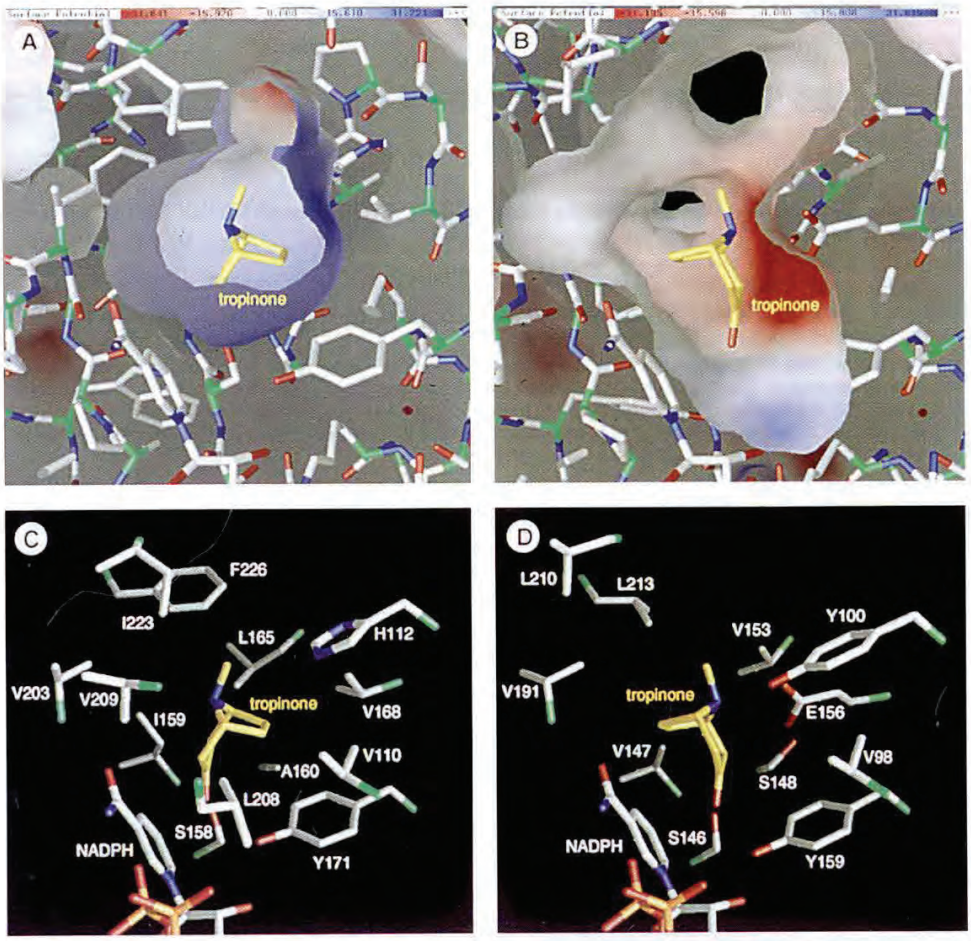

FIG. 5. Environments of the substrate binding sites and the binding models of tropinone. (*A* and *B*) Inner molecular surfaces of the tropinone binding pockets of TR-I (*A*) and TR-II (*B*). Electrostatic charge distributions are shown on the molecular surfaces in blue (positive charge) and red (negative charge). Note that the inner surface of TR-II (*B*) is somewhat deformed at the lower left corner due to the absence of several residues that constitute the small lobe. (*C* and *D*) Amino acid side chains that form the tropinone binding pockets viewed from the same direction as in *A* and *B*. Two TR-II residues (*D*) corresponding to the Leu-208 and Val-209 of TR-I (*C*) are missing in this structural model. Bonds from the carbon atoms in tropinone are shown in yellow, whereas the protein bonds from the Cα atoms are green to half their lengths. This figure was prepared by the GRASP program (23).

ated by Glu-156, which is replaced by the hydrophobic Val-168 in TR-I. As the nitrogen atom of tropinone is positively charged under physiological pH conditions (24), the charge distributions in the tropinone binding sites agreed well with the predicted orientations of tropinone. In TR-II, the orientation can be fixed in a straightforward manner: an acid–base interaction between the nitrogen atom of tropinone and the side chain of Glu-156. The relatively high affinity between TR-II and tropinone (K_m = 0.176 mM at pH 5.9; ref. 5) reflects this favorable interaction. In contrast, TR-I uses a rarely seen mechanism to orient tropinone, namely, repulsion between the positive charges of His-112 and the nitrogen atom of tropinone. Although this type of substrate recognition seems to be unfavorable in view of the affinity for tropinone, results from several biochemical experiments are consistent with this mechanism. The K_m of TR-I for tropinone is 0.775 mM at pH 5.9 (5), a value considerably higher than that of TR-II. This may be because of the inevitable exposure of the polar nitrogen atom of tropinone to the hydrophobic surface of the binding site (Fig. 5*A*). This high K_m value has been reported to be decreased by increasing the reaction pH (24), indicative that elimination of the positive charge from tropinone improves its affinity for TR-I. The same report also showed that 8-thiabicyclo[3,2,1]octane-3-one, a noncharged analog of tropinone could be reduced to either of the two possible stereoisomers by TR-I, indicating that the charged nitrogen atom is crucial for the strict stereospecificity. Moreover, the k_{cat} of TR-I is estimated to be about one order of magnitude higher than that of TR-II (5). The low affinity between the TR-I protein and tropinone (or tropine; refs. 1 and 24) may somehow act in favor of the rapid turnover of TR-I.

Apart from the charged residues described above, most of the amino acids that would contact tropinone within the binding sites are hydrophobic (Fig. 5 *C* and *D*). These residues would provide a favorable environment for the binding of tropinone, which generally has a hydrophobic nature. Although about half of these residues are replaced by different hydrophobic amino acids in the different TRs, comparison of the same TRs from different plant species (*H. niger*) restricted the enzyme type-specific replacements to two positions (Fig. 3, open arrowheads). Judged from their positions in the tropinone-binding sites, these residues are presumed to play only a minor role in orienting tropinone. Site-directed mutagenesis experiments are underway to obtain information on how each of these residues contributes to the stereospecificity.

Molecular Evolution. The structures presented herein are for a pair of enzymes that are closely related evolutionarily but which have different reaction stereospecificities. Comparison

Corteva Exhibit 2053 - Page 13 of 14
Bayer v. Corteva - IPR2023-01037

of the two TR structures made clear that opposite reaction stereospecificities can be acquired in enzymes that have a conserved overall folding, by changing the amino acids in the substrate binding site. A similar molecular evolution of acquiring different stereospecificity has been discussed for hydroxysteroid dehydrogenases (25). In other examples, creation of an enzyme with opposite stereospecificity appears to require a different protein framework under different circumstances. The overall folding of D-lactate dehydrogenase (D-LDH) and D-amino acid aminotransferase (D-AAT), for example, are completely different from those of the respective enzymes with normal stereospecificity (L-LDH and L-AAT) (11, 26). In these cases, the enzymes acting on the opposite stereoisomers are evolutionarily very distant from each other; only the active site structures have converged to form mirror images of each other. D-LDH is evolutionarily related to several D-2-ketoacid dehydrogenases that are widely distributed in nature (26). Evolution of D-LDH therefore may have been achieved more easily by altering the substrate specificity of a D-2-ketoacid dehydrogenase rather than switching the stereospecificity of L-LDH. Unlike lactate, tropinone has an intramolecular symmetry (*meso* form) and, hence, there is less need to drastically change TR's backbone framework for inverting its binding orientation. In the evolution of stereospecific enzymes, these alternative processes may have been chosen depending on the availability of preexisting protein folds that could best serve as a template for the new enzyme.

The refinement program was run on a computer at the Supercomputer Laboratory, Institute for Chemical Research, Kyoto University. This work was supported in part by grants from the Ministry of Education, Science, Sports and Culture of Japan (No. B07456049 to Y.Y.) and the Plant Cell Culture Technology Company, Japan.

1. Hashimoto, T., Nakajima, K., Ongena, G. & Yamada, Y. (1992) *Plant Physiol.* **100,** 836–845.
2. Nakajima, K., Hashimoto, T. & Yamada, Y. (1993) *Proc. Natl. Acad. Sci. USA* **90,** 9591–9595.
3. Nakajima, K., Hashimoto, T. & Yamada, Y. (1993) *Plant Physiol.* **103,** 1465–1466.
4. Jörnvall, H., Persson, B., Krook, M., Atrian, S., Gonzàlez-Duarte, R., Jeffery, J. & Ghosh, D. (1995) *Biochemistry* **34,** 6003–6013.
5. Nakajima, K., Hashimoto, T. & Yamada, Y. (1994) *J. Biol. Chem.* **269,** 11695–11698.
6. Furey, W. & Swaminathan, S. (1997) *Methods Enzymol.* **277,** 590–620.
7. Wang, B.-C. (1985) *Methods Enzymol.* **115,** 90–112.
8. Brünger, A. T. (1992) *X-PLOR Manual Version 3.1* (Yale Univ. Press, New Haven, CT).
9. Collaborative Computational Project, No. 4. (1994) *Acta Crystallogr. D 50,* 760–763.
10. Brünger, A. T., Krukowski, A. & Erickson, J. (1990) *Acta Crystallogr. A* **46,** 585–593.
11. Sugio, S., Petsko, G. A., Manning, J. M., Soda, K. & Ringe, D. (1995) *Biochemistry* **34,** 9661–9669.
12. Laskowski, R. A., MacArthur, M. W., Moss, D. S. & Thornton, J. M. (1993) *J. Appl. Crystallogr.* **26,** 283–291.
13. Kraulis, P. J. (1991) *J. Appl. Crystallogr.* **24,** 946–950.
14. Merritt, E. A. & Murphy, M. E. P. (1994) *Acta Crystallogr. D* **50,** 869–873.
15. Rossmann, M. G., Moras, D. & Olsen, K. W. (1974) *Nature (London)* **250,** 194–199.
16. Ghosh, D., Pletnev, V. Z., Zhu, D.-W., Wawrzak, Z., Duax, W. L., Pangborn, W., Labrie, F. & Lin, S.-X. (1995) *Structure* **3,** 503–513.
17. Nakanishi, M., Kakumoto, M., Matsuura, K., Deyashiki, Y., Tanaka, N., Nonaka, T., Mitsui, Y. & Hara, A. (1996) *J. Biochem.* **120,** 257–263.
18. Tanaka, N., Nonaka, T., Nakanishi, M., Deyashiki, Y., Hara, A. & Mitsui, Y. (1996) *Structure* **4,** 33–45.
19. Ghosh, D., Wawrzak, Z., Weeks, C. M., Duax, W. L. & Erman, M. (1994) *Structure* **2,** 629–640.
20. Tanaka, N., Nonaka, T., Tanabe, T., Yoshimoto, T., Tsuru, D. & Mitsui, Y. (1996) *Biochemistry* **35,** 7715–7730.
21. Breton, R., Housset, D., Mazza, C. & Fontecilla-Camps, J. C. (1996) *Structure* **4,** 905–915.
22. Oppermann, U. C. T., Filling, C., Berndt, K. D., Persson, B., Benach, J., Ladenstein, R. & Jörnvall, H. (1997) *Biochemistry* **36,** 34–40.
23. Nicholls, P. J., Sharp, K. A. & Honig, B. (1991) *Proteins Struct. Funct. Genet.* **11,** 281–296.
24. Portsteffen, A., Dräger, B. & Nahrstedt, A. (1994) *Phytochemistry* **37,** 391–400.
25. Bennett, M. J., Albert, R. H., Jez, J. M., Ma, H., Penning, T. M. & Lewis, M. (1997) *Structure* **5,** 799–812.
26. Stoll, V. S., Kimber, M. S. & Pai, E. F. (1996) *Structure* **4,** 437–447.

Corteva Exhibit 2053 - Page 14 of 14
Bayer v. Corteva - IPR2023-01037